

# Structure and Subunit Arrangement of the A-type ATP Synthase Complex from the Archaeon *Methanococcus jannaschii* Visualized by Electron Microscopy\*

Received for publication, June 3, 2004

Published, JBC Papers in Press, June 27, 2004, DOI 10.1074/jbc.M406196200

Ünal Coskun‡, Yuriy L. Chaban§, Astrid Lingl¶, Volker Müller¶, Wilko Keegstra§, Egbert J. Boekema§, and Gerhard Grüber‡¶

From the ‡Universität des Saarlandes, Fachrichtung 2.5-Biophysik, D-66421 Homburg, Germany, §Department of Biophysical Chemistry, Groningen Biomolecular Sciences and Biotechnology Institute, University of Groningen Nijenborgh 4, 9747 AG Groningen, The Netherlands, and ¶Institut für Mikrobiologie, Johann Wolfgang Goethe-Universität Frankfurt, D-60439 Frankfurt, Germany

In Archaea, bacteria, and eukarya, ATP provides metabolic energy for energy-dependent processes. It is synthesized by enzymes known as A-type or F-type ATP synthase, which are the smallest rotatory engines in nature (Yoshida, M., Muneyuki, E., and Hisabori, T. (2001) *Nat. Rev. Mol. Cell. Biol.* 2, 669–677; Imamura, H., Nakano, M., Noji, H., Muneyuki, E., Ohkuma, S., Yoshida, M., and Yokoyama, K. (2003) *Proc. Natl. Acad. Sci. U. S. A.* 100, 2312–2315). Here, we report the first projected structure of an intact  $A_1A_0$  ATP synthase from *Methanococcus jannaschii* as determined by electron microscopy and single particle analysis at a resolution of 1.8 nm. The enzyme with an overall length of 25.9 nm is organized in an  $A_1$  headpiece ( $9.4 \times 11.5$  nm) and a membrane domain,  $A_0$  ( $6.4 \times 10.6$  nm), which are linked by a central stalk with a length of  $\sim 8$  nm. A part of the central stalk is surrounded by a horizontal-situated rod-like structure (“collar”), which interacts with a peripheral stalk extending from the  $A_0$  domain up to the top of the  $A_1$  portion, and a second structure connecting the collar structure with  $A_1$ . Superposition of the three-dimensional reconstruction and the solution structure of the  $A_1$  complex from *Methanosarcina mazei* Gö1 have allowed the projections to be interpreted as the  $A_1$  headpiece, a central and the peripheral stalk, and the integral  $A_0$  domain. Finally, the structural organization of the  $A_1A_0$  complex is discussed in terms of the structural relationship to the related motors,  $F_1F_0$  ATP synthase and  $V_1V_0$  ATPases.

ATP synthases/ATPases are present in every life form and are the most important enzymes for the energy metabolism of the cell (1). They catalyze the formation of ATP at the expense of the transmembrane electrochemical ion gradient. They arose from a common ancestor that underwent structural and functional changes leading to three distinct classes of  $A_1A_0$ ,  $F_1F_0$ ,

and  $V_1V_0$  ATP synthases/ATPases. The V-type ATPases, found in organelles of eukaryotes, lost their ability to synthesize ATP. Their function is to create steep ion gradients at the expense of ATP hydrolysis (2). Archaea contain ATPases, the  $A_1A_0$  ATP synthases, that are structurally similar to  $V_1V_0$  ATPases but synthesize ATP like the F-type ATPases. The genomic sequences available today show that the overall subunit composition of the  $A_1A_0$  ATP synthases is very similar to the  $V_1V_0$  ATPases. For example, the  $A_1A_0$  ATP synthases contain duplicated and even triplicated K subunits (proteolipids) (3, 4). The  $A_1A_0$  ATP synthase has at least nine subunits ( $A_3B_3CDEFHK_X$ ), but the actual subunit stoichiometry, especially regarding the proteolipid subunits K in A ATPases, is different in various organisms (12, 6, 4, or as suggested by genomic data, only 1 (5)). The  $A_1A_0$  ATP synthase is composed of a water-soluble  $A_1$  ATPase and an integral membrane subcomplex,  $A_0$ . ATP is synthesized or hydrolyzed on the  $A_1$  headpiece consisting of an  $A_3B_3$  domain, and the energy that is provided for or released during that process is transmitted to the membrane-bound  $A_0$  domain (4). The energy coupling between the two active domains occurs via the so-called stalk part, an assembly proposed to be composed of the subunits C, D, and F (6, 7).

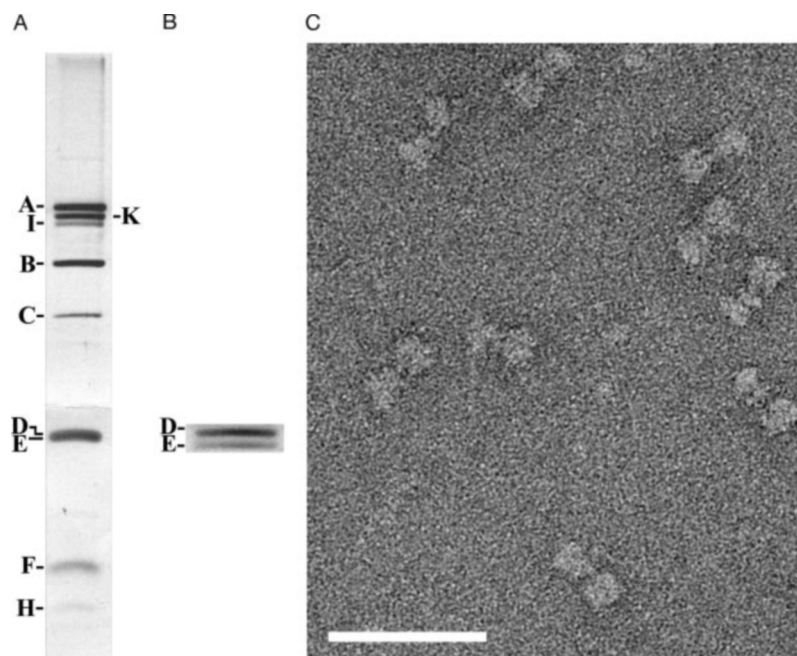
Insight in the molecular structure of the A-type ATP synthases comes from small-angle x-ray scattering data of the  $A_1$  ATPase from *Methanosarcina mazei* Gö1 whose  $A_1$  domain is made up of the five different subunits,  $A_3B_3CDF$  (8). The data have shown that the hydrated  $A_1$  ATPase is rather elongated with a headpiece of  $10 \times 9.4$  nm in dimension and a stalk of  $\sim 8.4$  nm in length. A comparison of the central stalk of this  $A_1$  complex with bacterial  $F_1$  and eukaryotic  $V_1$  ATPase indicates different lengths of the stalk domain (8, 9). Image processing of electron micrographs of negatively stained  $A_1$  ATPase from *M. mazei* Gö1 (7) has revealed that the headpiece consists of a pseudo-hexagonal arrangement of six masses surrounding a seventh mass. These barrel-shaped masses of  $\sim 3.2$  and 2.8 nm in diameter and 7.5 and 5.0 nm in length, which consist of the major subunits A and B, are arranged in an alternating manner (7). The hexagonal barrel of subunits A and B encloses a cavity of  $\sim 2.3$  nm in the middle in which part of the central stalk is asymmetrically located. The stalk protrudes from the bottom side of the headpiece forming an angle of  $\sim 20^\circ$  with the vertical axis of the molecule. At the upper end of the hexagonal barrel, extensions can be observed that are assumed to belong to the N termini of subunit A (7). Further insights into the topology of the  $A_1$  ATPase were obtained by differential protease sensitivity (8) and cross-linking studies (6, 7). These studies

\* This research was supported by Deutsche Forschungsgemeinschaft Grants GR 1475/9-1 and GR 1475/9-2 (to G. G.) and MU 801/10-3 (to V. M.) and from the Dutch Science Foundation NWO-CW Grant 99009 (to E. J. B.). The costs of publication of this article were defrayed in part by the payment of page charges. This article must therefore be hereby marked “advertisement” in accordance with 18 U.S.C. Section 1734 solely to indicate this fact.

¶ To whom correspondence should be addressed: Universität des Saarlandes, FR2.5-Biophysik, Universitätsbau 76, D-66421 Homburg, Germany. Tel.: 49-6841-162-6085; Fax: 49-6841-162-6086; E-mail: ggrueber@uniklinik-saarland.de.

<sup>1</sup> The abbreviations used are:  $A_1A_0$  ATPase, Archaea-type ATPase;  $F_1F_0$ ,  $F_1F_0$  ATP synthase;  $V_1V_0$  ATPase, vacuolar-type ATPase.

FIG. 1. SDS-PAGE of isolated  $A_1A_0$  ATP synthase from *M. jannaschii* and an electron micrograph of the negatively stained complex. A,  $A_1A_0$  ATP synthase was applied to SDS-PAGE (10%). To separate the subunits D (25 kDa) and E (23 kDa), the enzyme was loaded on a 17.5% gel (B). Both gels were stained with silver. The K-oligomer is SDS-resistant as shown recently (11) (C). Bar represents 50 nm.



resulted in a model in which the subunits C, D (partly), and F form the central stalk domain (7).

However, in contrast to the related F- and V-type ATP synthases/ATPases, little is known regarding the overall structure of the  $A_1A_0$  molecule, which is largely due to the instability of the isolated complexes (10). Most recently, an isolation procedure of the  $A_1A_0$  ATP synthase of the hyperthermophilic Archaea *Methanococcus jannaschii* resulted in a complete and functionally coupled enzyme (11). Besides the property of being an enzyme of a hyperthermophilic organism whose multienzyme complexes are believed to be more stable than those of mesophiles, the *M. jannaschii*  $A_1A_0$  ATP synthase is of particular interest because it has a K subunit three times the size of that of most bacteria and Archaea. Furthermore, this subunit has lost one of the ion translocating residues (12). Here, we used electron microscopy to visualize directly the structure of the  $A_1A_0$  ATP synthase from *M. jannaschii*. A comparison with the low resolution structure of the  $A_1$  ATPase from *M. mazei* Gö1, derived from small-angle x-ray scattering data and single particle electron microscopy, allowed the unambiguous identification of most of the densities in the stalk domain and the  $A_0$  part. The structure of the complete  $A_1A_0$  ATP synthase also facilitates, for the first time, a comparison with structural models of the related  $F_1F_0$  ATP synthase and  $V_1V_0$  ATPase holoenzymes.

#### EXPERIMENTAL PROCEDURES

**Materials**—All of the chemicals were of reagent grade and were obtained from Merck (Darmstadt, Germany), BIOMOL (Hamburg, Germany), Kral (Karlsruhe, Germany), or Sigma (Deisenhofen, Germany).

**Protein Preparation**—The  $A_1A_0$  ATP synthase of *M. jannaschii* was purified by sucrose density centrifugation and anion-exchange chromatography (DEAE-Sepharose) as described previously (11). ATPase-active fractions were pooled and concentrated on Centricon 100-kDa concentrators (Millipore). The concentrated sample was loaded on a Superose 6 column (10/30, Amersham Biosciences) and eluted with 50 mM Tris-HCl (pH 7.5), 5 mM MgCl<sub>2</sub>, 10% glycerine, 150 mM NaCl, 0.1% Triton X-100, 0.1 mM phenylmethylsulfonyl fluoride, and Pefabloc SC (a final concentration of 1 mM, BIOMOL). The peak fractions, which were stained with silver, were collected and analyzed by SDS-PAGE (13, 14). Mg<sup>2+</sup>-dependent ATPase activity was determined as described earlier (15).

**Electron Microscopy and Image Analysis**—Protein was prepared on freshly glow-discharged carbon-coated copper grids stained with 2%

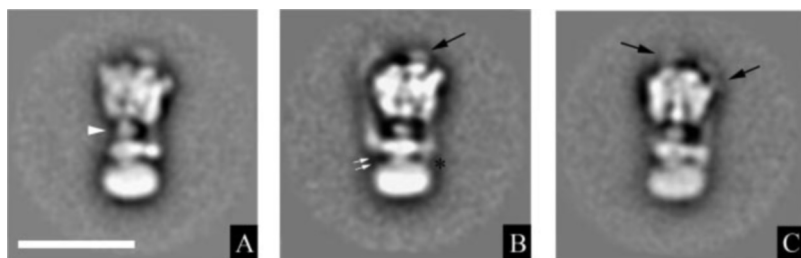
uranyl acetate. Images of the negatively stained  $A_1A_0$  ATP synthase were collected on a Philips CM20FEG electron microscope operating at 200 kV and liquid N<sub>2</sub>-cooled specimen to reduce radiation damage. Images of 2,048 × 2,048 pixels (after a binning of 2) were recorded at ×67,200 magnification at a pixel size of 30 μm with a Gatan 4000 SP 4K slow-scan CCD camera with GRACE software for semi-automated specimen selection and data acquisition (16). Single particle analysis was performed with the GRIP (Groningen image processing) software package on a PC cluster.<sup>2</sup> A total of 17,238 single particle projections (128 × 128 pixel frame; pixel size of 0.34 nm) from 331 images were obtained by selecting all of the discernable particles. For each micrograph, the defocus value was determined and a simple contrast transfer function correction by phase reversal was done (17). After band-pass filtering, the images were subsequently subjected to multireference alignment, multivariate statistical analysis, and hierarchical ascendant classification. This dataset was divided into two subsets including either one or two peripheral stalks to obtain a more homogenous dataset for a refinement of these classes. The subsets were analyzed in parallel by reference-free alignment (18). Each rotational and translational alignment was repeated four times, and classification was done by multivariate statistical analysis. Datasets were again divided and aligned as described above. The final classification of the homogenous datasets was performed by multivariate statistical analysis and hierarchical classification to extract the key structural features of the enzyme (19). The resolution of the class averages was measured according to van Heel (20).

#### RESULTS

**Subunit Composition and Electron Microscopy**—A characteristic gel of the preparation of the  $A_1A_0$  ATP synthase from *M. jannaschii* is presented in Fig. 1A showing the nine subunits, A–F, H, I, and K, with apparent molecular masses of 66, 51, 45, 25, 23, 11, 10, 77, and 21 kDa, respectively. A typical electron microscopy raw image of the enzyme yields monodisperse particles with almost no contamination by smaller particles that could represent dissociated complexes or fragments (Fig. 1B). A total of 17,238 such molecular images were subjected to image processing. Fig. 2 demonstrates different class sums of the  $A_1A_0$  ATP synthase projections obtained after several steps of reference-free translational/rotational alignment, multivariate statistical analysis, and multireference alignment. All of the projections reveal a tripartite structure consisting of a headpiece, a membrane-embedded domain, and a connecting stalk region. The classes can be grouped in respect

<sup>2</sup> W. Keegstra, unpublished data.

FIG. 2. A gallery of selected classes resulting from the last multivariate statistical analysis and classification of 17,238 particles of the  $A_1A_0$  ATP synthase. Four classes (1–4) showing either one (A) or two (B) peripheral stalk(s) besides the central stalk are shown.



to the number of visible stalks: one group showing one peripheral stalk besides the central stalk (Fig. 2, frames A1–4; 12,555 particles) and a second group with two peripheral stalks on both the left and right side (Fig. 2, frames B1–4; 4,683 particles). To obtain more homogeneous classes, both data sets, including either two or three stalks, were analyzed separately as described under “Experimental Procedures.” Fig. 3 shows averages of each refined data set at a resolution of 1.8 nm (Fig. 3, A–C). In all of the averages, the  $A_1A_0$  ATP synthase from *M. jannaschii* has a total length of 25.9 nm. The dimensions of the  $A_1$  headpiece, the central stalk domain, and the membrane portion,  $A_0$ , are  $9.4 \times 11.5$ ,  $8.0 \times 3.9$ , and  $6.4 \times 10.6$  nm, respectively. The  $A_1$  headpiece has a rather spherical mass that is clearly separated from the stalk domain at its base (Fig. 3B). The stalk domain is formed by a central stalk and either one (Fig. 3A) or two peripheral stalks (Fig. 3B). This observation might be explained either by some of the complexes being disrupted or by these classes containing complexes in different orientation. The central stalk can be divided into an asymmetric upper part and a collar-like structure located above the  $A_0$  domain. In the collar, several distinct densities could be resolved. At both ends of this domain, two of such densities are connected to the peripheral stalks (Fig. 3B), which go all the way up to the  $A_1$  headpiece. One of these stalks appears to be in close contact with two areas of the  $A_1$  headpiece with one located at the outside and the second located on top of the  $A_3B_3$  headpiece (Fig. 3, B and C). This peripheral stalk shows a clear connection to the  $A_0$  portion via the collar structure (Fig. 3, B and C). By comparison, the second peripheral stalk is attached to the top of the  $A_1$  headpiece (Fig. 3C) and extended slightly down from the collar domain (Fig. 3B). A corresponding weak density rises up from the  $A_0$  (Fig. 3B). Whereas the peripheral stalk(s) seems to be connected to the outside of the  $A_0$  domain, the central stalk is attached to the center of the membrane-embedded  $A_0$ , which appears as a rather symmetric flattened sphere and slightly tilted in most of the projections, especially in Fig. 2, frame B3.

**Localization of the Subunits Inside the  $A_1A_0$  ATP Synthase**—A known three-dimensional reconstruction of the asym-

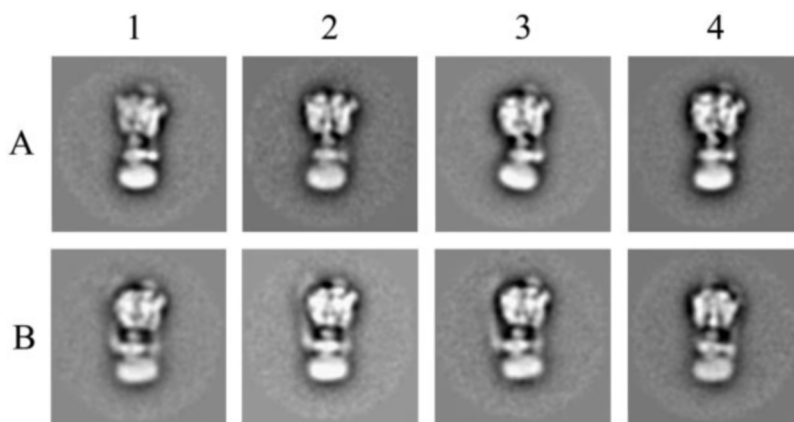


FIG. 3. Total averages calculated from 410 (A), 497 (B), and 316 (C) images. C, a projection at around  $40^\circ$  compared with that in B. Bar represents 20 nm. Labels: black arrows, masses of the peripheral stalks connected with the  $A_1$  headpiece; white arrowhead, asymmetric upper part of the central stalk; black asterisk, mass connecting the  $A_0$  with the collar like domain; white arrows, mass extending from the collar and the  $A_0$  domain.

metrical  $A_1$  complex from *M. mazei* Gö1 (7) determined from tilt pairs of negatively stained molecules was superimposed on the projection of the  $A_1A_0$  ATP synthase from *M. jannaschii* (Fig. 4, panel C) by rotating the  $A_1$  subcomplex in  $5^\circ$  steps through  $360^\circ$ . One of the projections of the  $A_1$  from *M. mazei* Gö1 is well accommodated within the  $A_1$  headpiece, composed of the  $A_3B_3D$  subassembly (7) and the upper central stalk, which is only partially (35%) solved in the three-dimensional reconstruction of the  $A_1$  ATPase from *M. mazei* Gö1 (7). In this projection, one of the catalytic A subunits is on the right of the  $A_1$  domain, implying that the peripheral stalk on the right may be close to this major A subunit. Nevertheless, from the superposition of the  $A_1$  profile with the  $A_1$  part in the  $A_1A_0$  ATP synthase images, it is clear that the cap at the top of the  $A_1$  headpiece (Figs. 3B and 4C) does not belong to the  $A_3B_3D$  subassembly. To further examine the composition of the central stalk, the projection of the  $A_1A_0$  ATP synthase from *M. jannaschii* was compared with the solution structure of the  $A_3B_3CDF$  complex of the  $A_1$  ATPase from *M. mazei* Gö1 deduced from solution x-ray scattering data (8). The central stalk of the hydrated  $A_3B_3CDF$  complex, which consists of the subunits C, F, and a part of subunit D, is 8.4 nm in length (8) and fits well to the dimensions (8 nm) of the elongated central stalk of the negative-stained  $A_1A_0$  ATP synthase, indicating that the central stalk is made up by the subunits C, D (partly), and F.

#### DISCUSSION

The  $A_1A_0$  ATP synthase has been described as a chimeric enzyme combining the structural and functional features of  $F_1F_0$  ATP synthases and  $V_1V_0$  ATPases (4). Single particle analysis resulted in the visualization of projections of the  $A_1A_0$  ATP synthase from *M. jannaschii* consisting of an  $A_1$  headpiece and an  $A_0$  domain linked by a central stalk and two peripheral stalks. The  $A_1$  headpiece fits well with the projection of the recently determined three-dimensional reconstruction with the  $A_1$  complex from *M. mazei* Gö1 composed of the hexagonal  $A_3B_3$  domain surrounding a cavity in which the central stalk subunit D is located (7, 8). The subunit is displaced toward an A-B-A triplet (7), allowing the rearrangements of the central D sub-



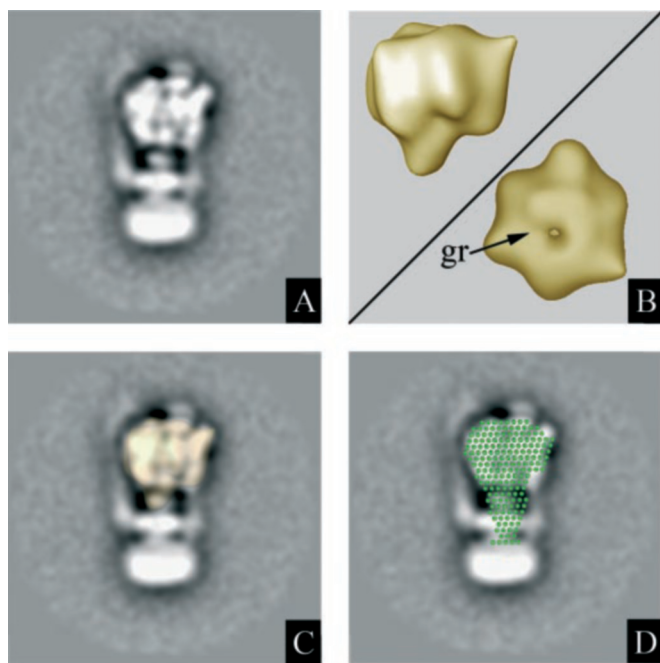


FIG. 4. A, C, and D, comparison of the  $A_1A_0$  ATP synthase from *M. jannaschii* (A) with the projection of the three-dimensional reconstruction of the  $A_1$  complex (C) (7) and the low resolution structure of the hydrated  $A_3B_3CDF$  complex (D) (8) from *M. mazei* G61. B, side and top view of the surface representation of the three-dimensional reconstruction of the  $A_1$  ATPase from *M. mazei* G61 at a 3.2-nm resolution (7). The black arrow points at the groove of the  $A_1$  headpiece. The side view of the  $A_1$  complex (gold; C) and the envelope of the hydrated  $A_3B_3CDF$  complex derived from small-angle x-ray scattering data (green; D) from *M. mazei* G61 are superimposed on the projection of the  $A_1A_0$  ATP synthase from *M. jannaschii*, respectively.

unit as demonstrated for the  $A_1$  ATPase from *M. mazei* G61 (6, 7) and the related *Thermus thermophilus*  $A_1V_1$  ATPase (21). A key feature from the superposition of the  $A_1$  complex from *M. mazei* G61 and the  $A_1A_0$  ATP synthase is the close fit at the top of the  $A_1$  headpiece showing the knoblike structures. These knobs, also found in the related V-type ATPase (22–25) but absent in the F-type ATP synthases (26–28), are formed by the N-terminal non-homologous inserts (80–90 amino acids) of the three catalytic A subunits, which alternate with the nucleotide-binding B subunits (7, 29). They point out that the cap at the very top of the  $A_1A_0$  molecule (Fig. 4C) is not formed by a subunit belonging to the soluble  $A_1$  domain (see below).

The comparison of the  $A_1A_0$  ATP synthase with the recently determined envelope of the *M. mazei* G61  $A_3B_3CDF$  complex in solution (8) yields that there is no significant shrinkage of the  $A_1A_0$  molecule through the negative staining procedure. The central stalk is rather elongated (~8 nm) and in close contact with  $A_0$ . As described recently, the central stalk of the *M. mazei* G61  $A_3B_3CDF$  complex accommodates subunits C, F, and partly D (7, 8). The cross-linking data of this complex indicate that subunit F is in close neighborhood to one of the nucleotide-binding B subunits (Fig. 5) and that F, together with the central stalk subunits C and D, undergoes significant structural rearrangements depending on nucleotide binding (6, 7). Such nucleotide-dependent alterations of stalk subunits C, D, and F will facilitate the mechanistic linkage of ATP synthesis/hydrolysis in the  $A_3B_3$  hexamer to ion pumping in the  $A_0$  part via the central CDF stalk domain. The length and the shape of the central stalk of the  $A_1$  part resemble those of the related  $V_1$  ATPase (8, 9). In contrast, the central stalk of the complete bacterial  $F_1$  ATPase is substantially shorter (4.0–4.5 nm) (9, 30).

The question that now arises is, which subunits of the  $A_1A_0$  ATP synthase contribute to the  $A_0$  domain, the peripheral

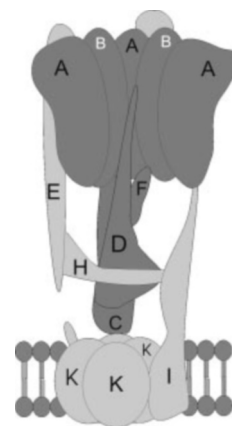


FIG. 5. Model of the subunit topology in the  $A_1A_0$  ATP synthase from *M. jannaschii*.  $A_1$  and  $A_0$  subunits are labeled in dark and light grey, respectively. The subunit topology in the A-type ATP synthase is based on biochemical (6–8) and structural data (Refs. 8, 9, and this work). The triplicated proteolipids of *M. jannaschii* arose by gene triplication followed by a fusion of the gene copies and resulting in the proposed stoichiometry of four K subunits (4).

stalks, and the additional mass on top of  $A_1$ . The  $A_1A_0$  ATP synthase as isolated has nine subunits (A–I, K). Five of them form the  $A_1$  part and are assembled in the stoichiometry  $A_3B_3CDF$  (see above). The I and K subunits form the membrane domain,  $A_0$  (11, 12). Subunit I (70 kDa) is very similar to subunit a of  $V_1V_0$  ATPases with a hydrophilic N-terminal and a hydrophobic C-terminal domain. The C terminus of subunit I is predicted to have seven transmembrane helices and is assumed to be functionally similar to subunit a of the  $V_1V_0$  ATPases and  $F_1F_0$  ATP synthases (3). The N-terminal domain is predicted to be highly  $\alpha$ -helical and assumed to be the functional homolog of the soluble domain of peripheral stalk subunit b of  $F_1F_0$  ATP synthases. Because only one of the peripheral stalks is clearly attached to the outside of the  $A_0$  domain, we conclude that the hydrophilic N terminus of subunit I emerges from the membrane-embedded  $A_0$  part and may go up along the side of  $A_1$  until the top of the  $A_1$  headpiece (Fig. 5). Whether the N-terminal domain might partly contribute to the cap on the top of the  $A_1A_0$  molecule can only be speculated. In the presented average, the peripheral stalk (right) has a kinked structure in the lower part, giving this domain the flexibility to wrap around the  $A_1$  headpiece and ending up as the cap on the top (Fig. 3, B and C). Insertion and deletion of altered length in the so-called “tether” domain of the peripheral stalk subunit b of the *Escherichia coli*  $F_1F_0$  ATP synthase, which is located above the membrane service, can be tolerated by the enzyme, indicating that this related connecting stalk has an inherent flexible structure (31). It has been suggested for the  $F_1F_0$  ATP synthases that flexibility of the domain might allow reorientation of the stalk to act as a stator for rotation in one direction during ATP synthesis and in the opposite direction during ATP hydrolysis (31, 32).

Subunit K is a homolog of the F-type subunit c with two transmembrane helices. It consists of fused tandem repeats of sequences corresponding to the F-type subunit. *M. jannaschii* has a subunit K with six membrane-spanning helices (27 kDa) but with only two active carboxylates per monomer (12), which are involved in ion conduction along the membrane. As in the case of the F-type ATP synthases (33, 34) and V-type ATPases (35), the K subunits (or c in the F- and V-type ATPases) are thought to form a ring, which belongs to the rotary element inside the  $A_1A_0$  ATP synthase. As shown in Fig. 4, the bottom of the central CDF-stalk domain spans the upper center of the  $A_0$  domain, facilitating the direct contact of the rotary ele-

ments, which consists of an ensemble made from the central stalk (CDF domain) and a ring of hydrophobic K subunits in the  $A_0$  membrane domain (21).

The second peripheral stalk appears to be connected to the collar domain and goes up to the  $A_1$  headpiece. Probable candidates for this stalk are the remaining  $A_1A_0$ -hydrophilic subunits H (12 kDa) and E (25 kDa) with the latter predicted to be highly  $\alpha$ -helical (12). The modest contact area of this peripheral stalk with the  $A_1$  headpiece, which is also evident in electron micrographs of the related bacterial  $V_1V_0$  ATPase from *Caloramator fervidus* (36), might be caused partially by stain accumulation. The top view projection of the rotated  $A_1$  complex (Fig. 4, panel D) shows a groove at the top of the  $A_3B_3$ -hexamer in close neighborhood to this peripheral stalk. Such a groove-like feature may form a binding domain for the peripheral connection in the  $A_1$  headpiece. In general, the positions of the peripheral stalks of the  $A_1A_0$  ATP synthase as deduced from side views cannot be directly verified from top view projections, because such projection are not present in significant numbers if intact  $A_1A_0$  molecules are prepared.

In summary, the first two dimensional projection maps of the  $A_1A_0$  ATP synthase from *M. jannaschii* presented provides the structural basis toward a fuller understanding of the mechanistic events occurring in this class of enzymes. The reconstruction at a 1.8-nm resolution shows similarities and diversities between the structural modules to the evolutionary-linked  $F_1F_0$  ATP synthases and  $V_1V_0$  ATPases, such as the catalytic  $A_1/F_1/V_1$  headpiece and the central stalk domain. Although the existence of one (26, 37) or two (27) peripheral stalk(s) in the  $F_1F_0$  ATP synthase is uncertain, these classes of ATPases/synthases might need at least one peripheral stalk acting as a stator that prevents the major hexameric arranged subunits ( $\alpha_3\beta_3$  or  $A_3B_3$ ) from following the rotation of the central stalk domain. Whether the visualized second peripheral stalk in the  $V_1V_0$  ATPase and in the presented  $A_1A_0$  ATP synthase might act as a regulatory domain in the A-type ATP synthase as described for the plant V ATPase (25) can now be addressed.

## REFERENCES

1. Yoshida, M., Muneyuki, E., and Hisabori, T. (2001) *Nat. Rev. Mol. Cell. Biol.* **2**, 669–677
2. Nelson, N. (1992) *Biochim. Biophys. Acta* **1100**, 109–124
3. Müller, V., Ruppert, C., and Lemker, T. (1999) *J. Bioenerg. Biomembr.* **31**, 15–28
4. Müller, V., and Grüber, G. (2003) *Cell Mol. Life Sci.* **60**, 474–494
5. Müller, V. (2004) *J. Bioenerg. Biomembr.* **36**, 115–125
6. Coskun, U., Grüber, G., Koch, M. H. J., Godovac-Zimmermann, J., Lemker, T., and Müller, V. (2002) *J. Biol. Chem.* **277**, 17327–17333
7. Coskun, U., Radermacher, M., Müller, V., Ruiz, T., and Grüber, G. (2004) *J. Biol. Chem.* **279**, 22759–22764
8. Grüber, G., Svergun, D. I., Coskun, U., Lemker, T., Koch, M. H. J., Schägger, H., and Müller, V. (2000) *Biochemistry* **40**, 1890–1896
9. Svergun, D. I., Konrad, S., Huss, M., Koch, M. H. J., Wiecezorek, H., Altendorf, K., Volkov, V. V., and Grüber, G. (1998) *Biochemistry* **37**, 17659–17663
10. Wilms, R., Freiberg, C., Wegerle, E., Meier, I., Mayer, F., and Müller, V. (1996) *J. Biol. Chem.* **271**, 18843–18852
11. Lingl, A., Huber, H., Stetter, K. O., Mayer, F., Kellermann, J., and Müller, V. (2003) *Extremophiles* **7**, 249–257
12. Ruppert, C., Kavermann, H., Wimmers, S., Schmid, R., Kellermann, J., Lottspeich, F., Huber, H., Stetter, K. O., and Müller, V. (1999) *J. Biol. Chem.* **274**, 25281–25284
13. Schägger, H., Cramer, W. A., and v. Jagow, G. (1994) *Anal. Biochem.* **217**, 220–230
14. Damerval, C., le Guillouix, M., Blaisomeau, J., and de Vienne, D. (1987) *Electrophoresis* **8**, 158–159
15. Heinonen, J. K., and Lahti, R. J. (1981) *Anal. Biochem.* **113**, 313–317
16. Oostergetel, G.T., Keegstra, W., and Brisson, A. (1998) *Ultramicroscopy* **74**, 47–59
17. Frank, J., and Penczek, P. (1995) *Optik* **98**, 125–129
18. Dube, P., Bacher, G., Stark, H., Mueller, F., Zemlin, F., van Heel, M., and Brimacombe, R. (1998) *J. Mol. Biol.* **279**, 403–421
19. van Heel, M., and Frank, J. (1981) *Ultramicroscopy* **6**, 187–194
20. van Heel, M. (1984) *Ultramicroscopy* **13**, 165–184
21. Imamura, H., Nakano, M., Noji, H., Muneyuki, E., Ohkuma, S., Yoshida, M., and Yokoyama, K. (2003) *Proc. Natl. Acad. Sci. U. S. A.* **100**, 2312–2315
22. Boekema, E. J., Ubbink-Kok, T., Lolkema, J. S., Brisson, A., and Konings, W. N. (1998) *Photosyn. Research* **57**, 267–273
23. Wilkens, S., Vasilyeva, E., and Forgac, M. (1999) *J. Biol. Chem.* **274**, 31804–31810
24. Grüber, G., Radermacher, M., Ruiz, T., Godovac-Zimmermann, J., Canas, B., Kleine-Kohlbrecher, D., Huss, M., Harvey, W. R., and Wiecezorek, H. (2000) *Biochemistry* **39**, 8609–8616
25. Domgall, I., Venzke, D., Luttgé, U., Ratajczak, R., and Böttcher, B. (2002) *J. Biol. Chem.* **277**, 13115–13121
26. Wilkens, S., and Capaldi, R. A. (1998) *Biochim. Biophys. Acta* **1365**, 93–97
27. Böttcher, B., Bertsche, I., Reuter, R., and Grüber, P. (2000) *J. Mol. Biol.* **296**, 449–457
28. Karrasch, S., and Walker, J. E. (1999) *J. Mol. Biol.* **290**, 379–384
29. Grüber, G., Wiecezorek, H., Harvey, W. R., and Müller, V. (2001) *J. Exp. Biol.* **204**, 2597–2605
30. Grüber, G. (2000) *J. Bioenerg. Biomembr.* **32**, 341–346
31. Grabar, T. B., and Cain, B. D. (2003) *J. Biol. Chem.* **278**, 34751–34756
32. Hardy, A. W., Grabar, T. B., Bhatt, D., and Cain, B. D. (2003) *J. Bioenerg. Biomembr.* **35**, 389–397
33. Stock, D., Gibbons, C., Arechaga, I., Leslie, A. G., and Walker, J. E. (2000) *Curr. Opin. Struct. Biol.* **10**, 672–679
34. Vonck, J., von Nidda, T. K., Meier, T., Matthey, U., Mills, D. J., Kühlbrandt, W., and Dimroth, P. (2002) *J. Mol. Biol.* **321**, 307–316
35. Wilkens, S., and Forgac, M. (2001) *J. Biol. Chem.* **276**, 44064–44068
36. Boekema, E. J., van Bremen, J. F. L., Brisson, A., Ubbink-Kok, T., Konings, W. N., Lolkema, J. S. (1999) *Nature* **401**, 37–38
37. Rubinstein, J. L., Walker, J. E., and Henderson, R. (2003) *EMBO J.* **22**, 6182–6192